MDPI

Article

Exploring *Xylella fastidiosa*'s metabolic traits using a GSM model of the phytopathogenic bacterium

Alexandre Oliveira [1,2,†], Emanuel Cunha [1,2,†], Miguel Silva [1,2], Cristiana Faria [1,2] and Oscar Dias [1,2*]

[1] Centre of Biological Engineering, University of Minho, 4710-057 Braga, Portugal
[2] LABBELS – Associate Laboratory, Braga, Guimarães, Portugal
* Correspondence: odias@deb.uminho.pt
† These authors contributed equally to this work.

Abstract: *Xylella fastidiosa* is a gram-negative phytopathogenic bacterium that caused a significant economic impact around the world. In the last decade, genome-scale metabolic models have become important systems biology tools for studying the metabolic behaviour of different pathogens and driving the discovery of novel drug targets. In this work, a GSM model of *X. fastidiosa* subsp. *pauca* De Donno was developed. The model comprises 1164 reactions, 1379 metabolites, and 508 genes. *in silico* validation of the metabolic model was achieved through the comparison of simulations with available experimental data. Aerobic metabolism was simulated properly and fastidian gum production rates predicted accurately. The GSM model allowed identifying potential drug targets, using a pipeline based on the model's gene essentially analysis.

Keywords: *Xylella fastidiosa*, GSM Modelling, iMS508, *merlin*, Drug Targeting.

Citation: Oliveira, A.; Cunha, E.; Silva, M.; Dias, O Exploring *Xylella fastidiosa*'s metabolic traits using a GSM model of the phytopathogenic bacterium. *Journal Not Specified* **2022**, *1*, 0. https://doi.org/

Received:
Accepted:
Published:

Publisher's Note: MDPI stays neutral with regard to jurisdictional claims in published maps and institutional affiliations.

Copyright: © 2022 by the authors. Submitted to *Journal Not Specified* for possible open access publication under the terms and conditions of the Creative Commons Attribution (CC BY) license (https://creativecommons.org/licenses/by/4.0/).

1. Introduction

Xylella fastidiosa is commonly known and widespread gram-negative phytopathogenic bacterium [1]. It usually resides in the xylem of its host and is then transmitted to other plants by insects that feed on the xylem-fluid [2]. Even though host specificity is a prevalent characteristic in many phytopathogenic bacteria [3], this is not the case of *X. fastidiosa*. According to the *Xylella spp*. host plant database [4], the infection has been recorded in over 500 plant species. Still, *X. fastidiosa*'s subspecies are rather host-specific and usually related to certain plant diseases [5,6]. One key characteristic of the infection caused by this phytopathogen is that some plants may be infected whilst not showing any symptoms [6]. Hence, an *X. fastidiosa* outbreak is significantly harder to mitigate.

The *X. fastidiosa* infection was first detected in European territory in the Apulia region of Italy and was caused by the *X. fastidiosa* subsp. *pauca* De Donno [7,8]. This led to a severe outbreak of a disease that would come to be known as olive quick decline syndrome. As a result, thousands of olive trees died, thus having a negative impact on the olive oil market and the local economy [8]. Future projections indicate, in a worst-case scenario, an economic impact of 5.2 billion Euros in Italy alone for the next 50 years [9]. Hence, *X. fastidiosa* was declared a quarantine pest by the European Commission, and was the highest-ranked crop infesting pest according to the Impact Indicator for Priority Pests (I2P2) metric, leading all the economic, social, and environmental ranked domains in 2019 [10].

With the rise in popularity of high-throughput sequencing techniques, the availability of genomic and metabolic data has been exponentially increasing. As a result, fields such as Systems Biology have gained significant relevance. Systems Biology aims at studying cells through a system-level approach, trying to uncover their structure and the dynamics between each of its components [11]. Genome-Scale Metabolic (GSM) Models are Systems Biology tools that combine both genomic and metabolic data for a given organism. Throughout the years these models have been extensively used to predict phenotypes for a given organism, under specific conditions, and to drive new knowledge of the metabolic

behaviour of the organism in study [12]. Moreover, GSM models are useful tools to unveil novel drug targets to kill pathogens with minimum effect on the host, leading to drug discovery or re-purposing [13,14].

In 2020, a GSM model of *X. fastidiosa* subsp. multiplex CFBP 8418 was published. That work aimed at developing a metabolic model to uncover metabolic characteristics connected to the fastidious growth of the phytopathogen [15]. Considering this, this work aimed at the reconstruction and validation of a GSM model of *X. fastidiosa* subsp. *pauca* De Donno, which is the cause of the olive quick decline syndrome [8]. This model is also to be compared against the subsp. multiplex CFBP 8418 model. Lastly, since there is no effective treatment for infected plants, the GSM model is to be used to investigate potential drugs that could be used as treatment, without affecting olive trees.

2. Materials and Methods

2.1. Software and Genome Files

The reconstruction process was supported by the metabolic models' reconstruction using genome-scale information (*merlin*) [16] framework. This software provides a friendly interface for genome annotation and manual curation, offering multiple features and plugins that accelerate the process. Furthermore, all simulations related to the final stage of reconstruction (model validation) were performed in COBRApy [17]. Lastly, the drug targeting pipeline performed in this work required both COBRApy and Biopython [18] packages.

X. fastidiosa subsp. *pauca* De Donno RefSeq assembly genome files, accessible via the NCBI [19] assembly accession number ASM211787v1 [20], were automatically retrieved with *merlin*.

2.2. Genome Annotation

The genome annotation of the genome of the bacterium was based on similarity searches with the basic local alignment search tool (BLAST) [21] against UniProtKB/SwissProt and UniProtKB/TrEMBL [**?**], setting an expected value (e-Value) of $1e^{-30}$ as the threshold.

The genome functional annotation was performed using the *merlin*'s "automatic workflow" tool, which annotates all candidate genes (a gene that has at least one of its homologous associated with a metabolic function) based on a set of defined organisms. The set and order of the organisms were based on phylogenetic proximity to *X. fastidiosa* and the number of records associated with the organism at UniProtKB/SwissProt.

Briefly, the workflow explores the list of retrieved homologous for each candidate gene, comparing it to the defined set of similar organisms. If a match is found, the candidate gene is automatically annotated with the enzyme commission (EC) number [22] and the product name of the closest organism's homologous gene. The employed automatic workflow is shown in Figure S1, along with the list of selected organisms.

2.3. Metabolic Network Reconstruction

2.3.1. Metabolic Data Integration

A draft metabolic network for *X. fastidiosa* was assembled by coupling the information obtained in the genome annotation step with metabolic data retrieved from the Kyoto Encyclopedia of Genes and Genomes (KEGG) database [23]. The EC numbers identified in the genome annotation step were used to select the reactions to be included in the draft network. Reactions involved in generic metabolic pathways, such as DNA methylation and rRNA modification, were ignored and not included in the model as these are unnecessary (modelling-wise) for the reconstruction process. To finalize the initial draft metabolic network, KEGG's spontaneous reactions were automatically added to the model.

2.3.2. Compartments

The subcellular compartment location of each protein was predicted using PSORTb 3.0 [24]. The resulting file was loaded into*merlin*, allowing the automatic integration of compartments into the model's reactions.

2.3.3. Transport Reactions

Transport reactions were generated using the Transport Systems Tracker (transyt.bio.di.uminho.pt). This tool, which is embedded in*merlin*, identifies genes in the organism's genome that encode transporter proteins and the respective substrate(s), using information available in The Transporter Classification Database [25]. Afterwards, it automatically creates and integrates transport reactions into the model with the respective gene association.

2.3.4. GPRs Associations

Gene-Protein-Reaction (GPR) represent relationships between genes, their encoding protein, and the respective enzyme's catalysed reactions. These associations are generally done using Boolean logic (AND/OR operators) and can represent promiscuous enzymes, isoenzymes, and enzymatic complexes. Additionally, GPR associations are extremely valuable for high-quality GSM model reconstructions, as mutant phenotype predictions are heavily dependent on them.

Determining GPR associations can be a time-costly process as it requires extensive literature and biological database search. Therefore, here a tool that retrieves information from KEGG BRITE regarding the protein's structure available in *merlin* was used to automatically generate GPR rules. Subsequently, the formulated GPRs were manually curated (if necessary) or inserted for manually created reactions.

2.3.5. Biomass and Energy Requirements

The *Escherichia coli* GSM model (iOJ1366) [26] and *Xanthomonas campestris* large-scale metabolic model [27] were used as templates to infer the macromolecular composition of the biomass equation. This information was complemented with data retrieved from the literature.

The biomass reaction accounts for a total of seven macromolecular entities, namely Deoxyribonucleic acid (DNA), Ribonucleic acid (RNA), Protein, Cofactor, Peptidoglycan, Lipopolysaccharide, and Lipid. Deoxynucleotide, nucleotide, and amino acid contents were determined through *merlin*'s e-Biomass tool [28]. Additionally, this tool formulated a template reaction for the Cofactor macromolecule, which was promptly rearranged considering the metabolic potential of the assembled metabolic network. However, as the composition of the remaining macromolecules cannot be obtained through genomic information, available literature was sought to determine the necessary precursors for the synthesis of peptidoglycans [29], lipopolysaccharides [30,31] and lipids [32]. Finally, as the lipidic portion of the biomass requires fatty acids for its synthesis, whose chain is of variable size, an average fatty acid metabolite was created based on data of multiple strains of *X. fastidiosa* [1] as described elsewhere [33].

Growth and non-growth associated energy requirements were included in the model, as these represent the energy required for several cellular processes, including the assembly of macromolecules and the maintenance of internal homeostasis. As there is a lack of information regarding energy requirements for *X. fastidiosa*, information from the iOJ1366 model was adapted to this work. Therefore, growth-associated energy necessities, represented in the biomass equation, were set as the consumption of 53.5 $mmol \cdot g_{DW}^{-1}$ of ATP. Likewise, non-growth associated requirements were defined through an ATP hydrolysis reaction, while setting its lower and upper bounds to 3 $mmol \cdot g_{DW}^{-1} \cdot h^{-1}$.

2.4. Manual Curation

To accurately represent an organism's metabolic behaviour, manual curation is required. Therefore, whenever in silico simulations did not corroborate experimental data, manual curation of the GSM model was carried out.

2.4.1. Reversibility and Directionality

All reactions in the initial assembled network were set as reversible, as this is the default status set in KEGG. Therefore, a preliminary reversibility/directionality correction was performed automatically within*merlin*, according to information of Zeng's database [34]. However, model feasibility was unattainable and manual curation had to be performed. BiGG (Schellenberger et al., 2010), MetaCyc (Karp et al., 2000), and BRENDA (Schomburg et al., 2002) were crucial for determining the correct direction and reversible status of multiple reactions in this stage, while ModelSEED (Henry et al., 2010) and eQuilibrator (Flamholz et al., 2012) were used to a lesser extent. Furthermore, when in doubt, the template models (*E. coli* and *X. campestris*) were accessed to retrieve information related to the directionality/reversibility of reactions.

2.4.2. Gap-Filling

Dead-end metabolites and blocked reactions were identified using *merlin*.

Through this phase, an initial assessment of the metabolic potential of *X. fastidiosa* was performed by reviewing organism-specific literature. Specifically, pathways with metabolic gaps were evaluated to a higher degree. Furthermore, whenever a gap was found, supporting evidence at the genome level was sought, in the information obtained from the genome annotation step. If the enzyme that catalyses the missing reaction was indeed encoded in the genome, such reaction, and its associated GPR rule, was added to the model. Thus, multiple missed/misannotations were corrected during this comprehensive analysis.

Moreover, a tool recently added to the*merlin* software, BioISO [35], was also used during this process. BioISO tests the capability of the network towards the synthesis of products of a given reaction. Therefore, this tool is very valuable to test the network potential to produce biomass precursor molecules and can pinpoint potential issues within the network for the users.

2.5. Model Validation

The reconstructed GSM model's performance was evaluated by comparing the predicted results to available information retrieved from the literature. As there is a limited amount of information regarding *X. fastidiosa* metabolism, *X. campestris* data were used whenever necessary. In this work, all *in silico* simulations were made by setting one of the biomass reactions ('R_e-Biomass' or 'R_Coupled_Biomass') as the objective function and maximizing it using Parsimonious Flux Balance Analysis (pFBA) [36], except otherwise indicated. Finally, multiple metabolic properties were tested (described in the sections below) by restraining the model properly.

2.5.1. Aerobic Metabolism

As first described by Wells *et al.* [1], *X. fastidiosa* is a strictly aerobic bacterium. Hence, the aerobic metabolism of the phytopathogen's was evaluated, accounting for two different conditions. Specifically, an aerated environment was simulated by leaving the oxygen exchange reaction unbounded, while in an anaerobic condition the reaction's lower bound is set at a value of 0 $mmol \cdot g^{-1} \cdot h^{-1}$. In addition, glucose was provided as a carbon source and all amino acids were available for uptake in both conditions.

2.5.2. Amino Acid Auxotrophies

Amino acid auxotrophies were tested by allowing all amino acids to be consumed from the medium. Subsequently, one simulation per amino acid omission was performed.

If the growth rate is equal to zero the amino acid was essential for growth, and thus the organism is auxotroph for the amino acid.

2.5.3. Glucose Flux Pattern

Glucose flux pattern through the assembled metabolic network was assessed to allow direct comparison to *X. campestris* experimental data. Therefore, an environmental condition that replicates a minimal medium was formulated, where glucose and ammonia were used as carbon and nitrogen sources, respectively. Additionally, flux through the phosphofructokinase reaction (R00764, EC 2.7.1.90) was restrained to a minimal value (1% of the glucose intake rate), as the pyrophosphate-dependent phosphofructokinase identified in *X. fastidiosa*'s genome displays low processivity and represents a minimal fraction of the total proteome in similar organisms [27,37,38].

A quantitative validation was performed by evaluating the GSM model's predicted growth and exopolysaccharide production rates. However, as there is limited information related to this topic for *X. fastidiosa*, both data published alongside the large-scale metabolic model of *X. campestris* [27] and reported by Letisse *et al.* [39], were used for validation purposes.

Nonetheless, the environmental conditions had to be properly constrained, identically to previous validation steps, as the data retrieved from *X. campestris* concerns its growth under sucrose, an absent metabolite in the reconstructed GSM model of *X. fastidiosa*. As a result, glucose was used as a carbon source, instead of sucrose, and the carbon intake was normalized according to the number of carbon atoms (an uptake rate of 1.8 $mmol \cdot g^{-1} \cdot h^{-1}$ of sucrose equals an uptake rate of 3.6 $mmol \cdot g^{-1} \cdot h^{-1}$ of glucose).

2.5.4. Comparison with *X. fastidiosa* subsp. multiplex CFBP 8418 GSM Model

For validation purposes, the model developed in this work was directly compared to the GSM model of *X. fastidiosa* subsp. multiplex CFBP 8418 [15]. The first comparison relied on the minimization of glutamine uptake a predefined set of growth, exopolysaccharide production and LesA (a protein secreted by *X. fastidiosa*) production rates. This last entity, a lipase/esterase known to be secreted by *X. fastidiosa* and a key virulence factor during the phytopathogen's infection process [40], was inserted in the model by creating a biosynthetic reaction that accounted for its amino acid composition.

Distinct carbon sources were tested to examine whether they supported *X. fastidiosa*'s growth. Hence, the environmental conditions replicated a minimal medium, where ammonia, orthophosphate and Fe^{2+} would act as sources of nitrogen, phosphate, and iron, respectively. Additionally, carbon uptake was normalized according to the number of carbon atoms of the carbohydrate. Simulation outputs were then compared to Biolog Phenotype Microarray data, published along with a GSM model of *X. fastidiosa* subsp. multiplex CFBP 8418.

2.6. Identification of Potential Drug Targets

One of the most important applications of the *X. fastidiosa*'s reconstructed GSM model is the identification of potential drug targets that could impair the organism's survival. Nevertheless, high-quality GPR associations alongside correctly formulated environmental conditions are required for a significant critical genes analysis. A medium based on the olive tree's xylem fluid chemistry [41], was replicated as it would reflect the natural environment of the phytopathogenic bacterium. Additionally, a chemically defined media, CHARD2 [42], which replicates the xylem environment was also used in this step.

To identify potential drug targets, the model's essential genes were determined using the adequate methods available in COBRApy. The determined genes were filtered using a simple pipeline, which included a BLAST (e-Value threshold of 0.0001) against the available *Olea europaea* genome for each of the critical genes and evaluated if significant homologues were identified. However, before discarding a gene as a potential drug target because homologues genes were found in the host's genome, a metabolic potential analysis of the

host, using KEGG and MetaCyC pathways as an information source, was performed to evaluate the possibility of alternative metabolic routes for the same objective. In other words, if a reaction encoded by an *in silico* essential gene was essential for *X. fastidiosa* but not for the host (*Olea europaea*), the gene could be considered as a potential drug target and focused for further analysis. Finally, DrugBank was used to find potential inhibitors of the filtered genes. BLAST searches and the analyses of EC numbers associated with each gene were performed against this database. Only compounds classified as inhibitors or antagonists were included. Then, using information retrieved from DrugBank [43] and BRENDA [44], the collected compounds were filtered to include only drugs with known activity in gram-negative bacteria.

Furthermore, to find other strategies to possibly kill the phytopathogenic organism, synthetic lethal, which are pairs of non-essential genes whose simultaneous knockout leads to model infeasibility towards biomass maximization, and triple gene knockout *in silico* simulations were performed.

3. Results and Discussion

3.1. Genome Annotation

The genome annotation of *X. fastidiosa* subsp. *pauca* De Donno's identified a total of 825 candidate genes, 88% of them having hits to SwissProt's database. As stated in the previous section, an automatic workflow was employed in the genome annotation procedure. As a result, about 46% of the candidates were annotated based on hits from *Xylella spp.*, reflecting a high-quality and trustworthy genome annotation of the organism. A more detailed description of the genome annotation results is presented in Table S2.

Out of the 825 candidate genes, a total of 735 were identified as metabolic (associated with an EC number). Therefore, the genome annotation identified around 35% of the genome of *X. fastidiosa* subsp. *pauca* De Donno as metabolic genes. Several reasons led to a decrease in the number of genes included in the metabolic model, including genes that encode enzymes with irrelevant metabolic processes from a metabolic model perspective. Moreover, it also includes genes related to DNA and RNA processes, misannotations identified during manual curation, and genes annotated with incomplete EC numbers, which represent 16% of the overall metabolic genes. Nevertheless, when relevant KEGG reactions were associated with incomplete EC numbers, the respective genes could still be added to the model. For instance, after the annotation process, B9J09_RS08675 was associated with the EC number 2.7.8.-. Despite the incomplete EC number, the gene is known to be associated with a reaction necessary for cardiolipin synthesis. Thus, both the reaction and gene were included in the model.

3.2. Biomass and Energy Requirements

The macromolecular composition of the *X. fastidiosa*'s model reconstructed in this work, whose entities and respective fractions were inferred from *E. coli* [26] and *X. campestris* [27] models, is compiled in Table 1. A detailed biomass composition is available in Table S1.

Due to the phylogenetic closeness between *X. campestris* and *X. fastidiosa*, most biomass-relative contents were directly retrieved from the former model, whenever possible. Data from *E. coli* was used to determine the remaining macromolecular contents, but the missing portion of *X. campestris* was always considered during the calculations.

Despite the usage of glycogen in iOJ1366 [26] and *X. campestris* [27] models, the macromolecule was not added to the biomass equation of the *X. fastidiosa* model, as the glycogen metabolism seems to be a lost trait in multiple parasitic bacteria, including *X. fastidiosa* [45]. This was further confirmed by the lack of biosynthetic and catabolic enzymes related to glycogen during the genome annotation step. Nevertheless, the glycogen fraction was divided in a $30 - 70\%$ split and allocated into peptidoglycan and lipopolysaccharide, as both these macromolecules contain carbohydrates in their constitution. DNA, RNA and Protein compositions, in terms of precursors, were determined using the e-Biomass tool [28], which is embedded in*merlin*.

Table 1. Biomass equation representing the macromolecular composition of *X. fastidiosa* (this work), *E. coli* [26] and *X. campestris* [27] models. The fraction of each macromolecule is represented in grams of molecule per gram of cell dry weight.

Macromolecule	*E. coli*	*X. campestris*	*X. fastidiosa*
DNA	0.031	0.040	0.040
RNA	0.205	0.160	0.160
Protein	0.550	0.490	0.490
Lipid	0.091	0.130	0.130
Glycogen	0.025	-*	-
Peptidoglycan	0.025	-	0.0589
Cofactor	0.039	-	0.0706
Lipopolysaccharide	0.034	0.033	0.0505

*Altough glycogen was not included in the biomass reaction, it's production was constrained to a ratio of 2.21 glycogen/biomass.

Peptidoglycan production was represented by creating a reaction that accounted for all of its precursors. As *X. fastidiosa*'s peptidoglycan data is still lacking, information from *E. coli* [29] was retrieved to formulate peptidoglycan biosynthesis, which is composed of two monosaccharide units and five amino acids. One of these amino acids is D-Glutamate, which was promptly replaced by the enantiomer L-Glutamate as *X. fastidiosa*'s metabolic network could not support its biosynthesis.

The lipidic portion of the biomass, which comprises membrane phospholipids, was adapted from data of *X. campestris* B-24 [32], as no information was available for *X. fastidiosa*. Phosphatidylinositol and lysophosphatidylethanolamine, compounds measured in the previous experiment, were ignored since these were not found in the assembled *X. fastidiosa*'s metabolic network. Therefore, these lipidic contents were distributed among the other phospholipids. LPS, a constituent of gram-negative bacterial outer membranes, is composed of three moieties: Lipid A, core oligosaccharide and O-antigen. While the Lipid A and the inner portion of the core oligosaccharide are conserved in different bacterial species, both the core oligosaccharide's outer section and the O-antigen, which is an important virulence determinant, are structurally variable [30,31]. These structural changes were inferred from data published by [29] and an LPS synthesis reaction specific for *X. fastidiosa* was assembled.

The remaining biomass portion was associated with the e-Cofactor macromolecule, which is first determined using the e-Biomass tool [28]. However, a rearrangement was performed according to the metabolic potential of the network. As no information regarding the amount of each molecule in the cofactor pool is available, it was assumed that each cofactor would have the same weight (in grams) in the final biomass formulation.

The inclusion of energy requirements, which include both cell growth and maintenance-related energy, completed the *X. fastidiosa*'s biomass formulation. As stated previously, energy necessities were retrieved from the iOJ1366 *E. coli* model [26].

Due to the possibility of exopolysaccharide biosynthesis during the life cycle of *X. fastidiosa*, a reaction that couples biomass and exopolysaccharide production was inserted in the model ("R_Coupled_Biomass"), as these entities would compete for the available carbon source. This reaction forces the synthesis of biomass and fastidian gum (*X. fastidiosa*'s exopolysaccharide) as follows: 0.203 Biomass+0.797 Fastidian gum=>1.0 Coupled Biomass.

The stoichiometries were inferred from published data for *X. campestris* [46], and employed in the large-scale metabolic model of *X. campestris* [27].

3.3. Model Validation

An assessment of the aerobic metabolism of *X. fastidiosa* was the first validation step performed in the developed GSM model. As expected, the pathogen's model shows biomass production in an aerated environment and infeasible solutions when oxygen

is restricted. The infeasible solutions are explained by the fact that even the energetic maintenance requirements failed to be fulfilled. Hence, the aerobic metabolism observed *in vivo* was properly simulated, as the organism does not survive without oxygen. Moreover, as expected, the model's simulations revealed flux through the reactions catalysed by the enzymatic complexes associated with the oxidative phosphorylation, namely, NADH dehydrogenase, succinate dehydrogenase, ubiquinol oxidase and ATP synthase.

The next step was to validate for amino acid auxotrophies. To the best of our knowledge, no auxotrophies for *X. fastidiosa* were documented in the literature. This indicates that the phytopathogen is apparently able to grow using exclusively glutamine as a nitrogen source [47]. Hence, since the bacterium resides in limited nutrient environments, it is expected that the model for *X. fastidiosa* ought to be able to synthesize all amino acids. In this validation process, single amino acid omissions were performed revealing no auxotrophies, in compliance with the reported data.

3.4. Model Summary

The GSM model reconstructed in this work, comprises a total of 508 genes, 1379 metabolites and 1164 reactions, whose distribution can be seen in Figure 2. This model also includes 1014 GPR associations, 241 transport reactions, and 90 exchange reactions. The iMS508 model is available in the BioModels database [48] (MODEL2205020002) in Systems Biology Markup Language (SBML) version 3 format [49].

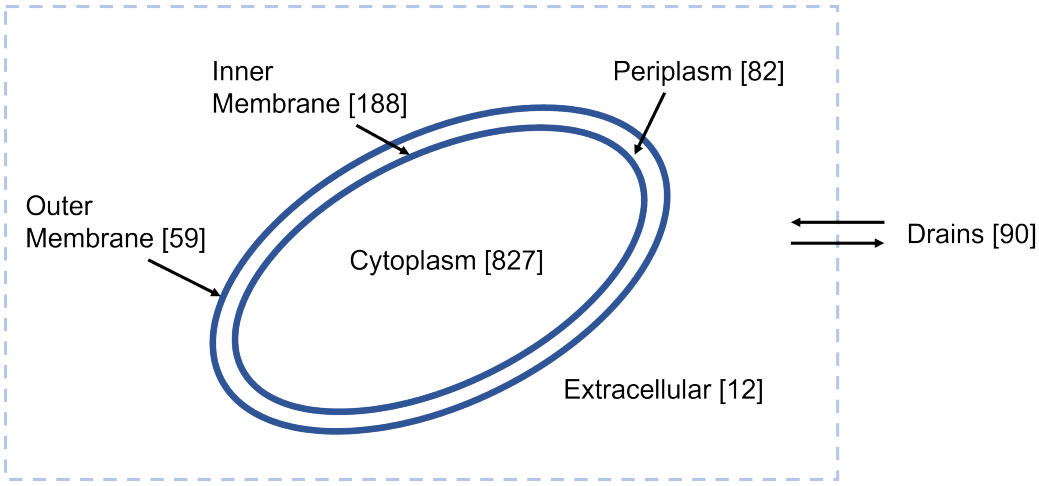

Figure 1. Summary of the distribution of reactions among the different compartments in the iMS498 model, which accounts for a total of 1164 metabolic reactions and 90 drains.

3.5. Glucose Flux Pattern

Several xanthomonads use the Entner-Doudoroff pathway (EMP) as the main catabolic route for glucose [50], including *X. campestris* [38]. Although this was not demonstrated for *X. fastidiosa* yet, due to the genetic and metabolic similarities among these organisms, the EMP has been proposed to be the main glucose degradation pathway for *X. fastidiosa* [51].

By assuming the maximisation of biomass production, the model predicts 88.6% and 8.6% of the glucose flux towards the Entner-Doudoroff and the non-oxidative branch of the pentose phosphate pathways, respectively (Figure **??**), which is in the range of the experimental data available for other organisms: $81 - 93\%$ and $7 - 19\%$ [50].

X. fastidiosa seems to present a pyrophosphate-dependent phosphofructokinase (EC 2.7.1.90), similar to the one identified in *X. campestris* [37]. An ATP dependent phosphofructokinase was not found in the genome annotation of *X. fastidiosa*. This could explain a flux bottleneck through the glycolytic pathway, as the pyrophosphate-dependent phosphofructokinase is less efficient than the ATP dependent enzyme [37]. Furthermore, phosphofructokinase deletion mutants of *X. campestris* are unaffected when compared

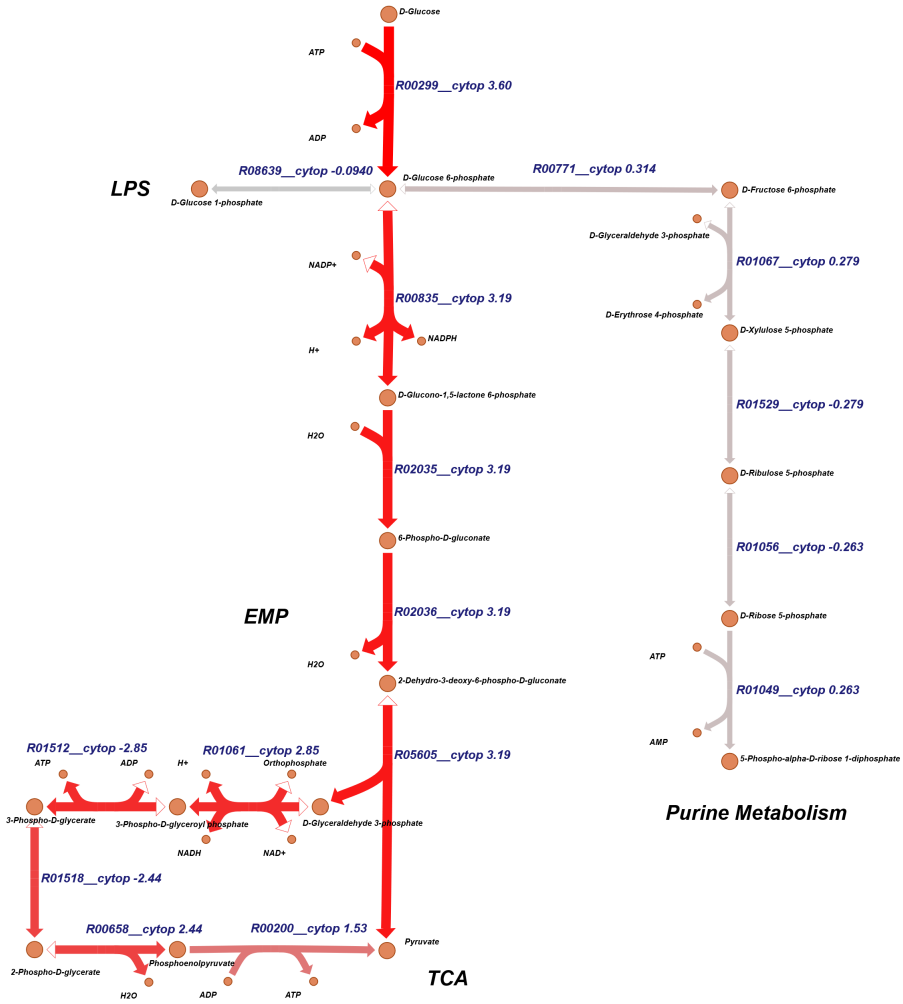

Figure 2. Glucose catabolism obtained from a pFBA simulation.

with the wild type [27]. Previous studies indicated the impossibility of this organism to use gluconeogenesis, due to the lack of fructose-1-6-bisphosphatase (EC 3.1.3.11) [52]. The pyrophosphate-dependent phosphofructokinase could close this gap found in the gluconeogenic pathway, as there is not a preferred direction of the reaction catalysed by the enzyme [37]. Moreover, according to *in silico* simulations, gluconeogenesis is mandatory when organic acids and amino acids, which are usually available in a xylem fluid environment [53], are used as carbon sources for *X. fastidiosa*'s growth.

Plant cells can produce reactive oxygen species (ROS) in response to environmental stress, including the invasion by pathogenic organisms [54]. Additionally, ROS levels are substantially increased to act as defence mechanisms to fight off invasive pathogens [52]. Therefore, the usage of Entner-Doudoroff as a catabolic pathway for carbohydrates could offer a metabolic advantage in comparison to glycolysis, as the pathway generates NADPH, which is especially meaningful in the detoxification of ROS. For instance, a study performed with *Pseudomonas putida*, known to catabolise carbohydrates through the Entner-Doudoroff pathway, shows that the organism is highly tolerant against oxidative stress, while a transgenic strain with activated glycolysis becomes sensitive to ROS [55]. Therefore, *X. fastidiosa* may use the Entner-Doudoroff pathway as a source of redox potential as means to act against plant defence mechanisms.

3.6. Specific growth rate and exopolysaccharide production

Specific growth and exopolysaccharides production rates were directly compared with *in silico* simulations of the *X. campestris* large scale metabolic model [27] and experimental data of the aforementioned species [39]. *X. fastidiosa* subsp. *pauca* De Donno GSM model was properly constrained to be possible to perform this direct comparison. Therefore, glucose was used for the *in silico* simulations of the model developed in this work.

As displayed in table 2, the model *X. fastidiosa* predicted a growth rate value of 0.11 h^{-1} and a specific production rate of exopolysaccharide of 0.44 $mmol \cdot g^{-1} \cdot h^{-1}$. The results are similar to the experimental data [39] and agree with the known fact that *X. fastidiosa* displays slower growth and exopolysaccharide production rates in comparison to *X. campestris*.

Table 2. *In silico* predictions of growth and exopolysaccharide production rates for *X. fastidiosa* iMS508, and *X. campestris* [27] metabolic models, in comparison to experimental data specific for *X. campestris* [39].

Source	**Growth Rate (h^{-1})**	**Exopolysaccharide Production ($mmol.g^{-1}.h^{-1}$)**
X. fastidiosa	0.11	0.44
X. campestris	0.12	0.47
X. campestris (exp. data)	0.13	0.52

The other end-products of *X. fastidiosa* subsp. *pauca* De Donno GSM model *in silico* simulations were assessed. As expected, the major outputs are water and carbon dioxide, which are by-products of the respiration metabolism. On the other hand, xanthomonadin was predicted to be produced at a small rate. Note that these metabolites were inferred to be produced by the organism after an analysis of the metabolic capabilities of the assembled network. Firstly, xanthomonadins are yellow pigments with photobiological damage protection properties produced by *Xanthomonas spp.* [56]. Since *X. fastidiosa* lacks a transaldolase (EC 2.2.1.2), D-Erythrose-4-phosphate can not be completely recycled by the organism; hence, xanthomonadins production was inferred. According to the metabolic model, D-Erythrose-4-phosphate could only be metabolised in the shikimate pathway and, as a result, dead-end metabolites of this pathway were thoroughly analysed. Evidence found shows that chorismate was linked to the synthesis of both ubiquinone and xanthomonadin through a bifunctional chorismatase [57] found in *X. fastidiosa*'s genome. Therefore, we assumed the production of xanthomonadin and added the necessary reactions.

3.7. Comparison with X. fastidiosa multiplex CFBP 8418 GSM model

Recently, a GSM model of *X. fastidiosa* multiplex CFBP 8418 was published [15]. Therefore, the two metabolic models were compared to assess metabolic differences between the two strains. A topological comparison between the models is displayed in Table 3, and as it can be seen, the models show a small difference in the number of genes, metabolites, and reactions.

Table 3. Comparison of the number of genes, metabolites and reactions between the GSM models of *X. fastidiosa* subsp. *pauca* De Donno (this work) and *X. fastidiosa* multiplex CFBP 8414 [15].

	***X. fastidiousa pauca* De Donno**	***X. fastidiousa* multiplex CFBP 8418**
Genes	508	572
Metabolites	1285	1107
Reactions	1164	1158

Subsequently, a minimisation of L-glutamine uptake, while restraining the growth rate, EPS and LesA production to a specific output, was performed and compared to the

published data. As displayed in Table 4, the uptake of L-glutamine and other metabolites was identical, and the discrepancies can be explained by the intrinsic details of the biomass assembly reaction of each model. Additionally, the composition of the LesA protein is different in these two models; however, the prediction results do not show any significant difference between both models.

Table 4. Simulation performance between the two *X. fastidiosa's* GSM models, in minimisation of L-glutamine intake situation.

Intake	***X. fastidiosa pauca* De Donno**	***X. fastidiosa* multiplex CFBP 8418**	**Output**	***X. fastidiosa pauca* De Donno**	***X. fastidiosa* multiplex CFBP 8418**
	Uptake flux ($mmol.g^{-1}.h^{-1}$)			Output flux ($mmol.g^{-1}.h^{-1}$)	
Oxygen	25.45	26.31	CO_2	33.64	33.83
L-Glutamine	15.65	16.24	NH_3	28.35	28.99
Phosphate	1.44	1.44	H_2O	2.78	2.60
Sulfate	0.067	0.064	EPS	1.296	1.296
Fe^{2+}	0.0012	0.0014	Biomass	0.1608	0.1608
-	-	-	LesA	0.0024	0.0024

A comparison to evaluate the usage of different carbon sources by *X. fastidiosa* was then performed. The results revealed different behaviours between both models for a subset of the tested carbon sources (Figure 3). While *X. fastidiosa* subsp. *pauca* De Donno GSM model only predicts growth for 14 out of the 24 tested carbon sources, the *X. fastidiosa* multiplex CFPB 8414 GSM model simulates growth in all of them. *In silico* simulations of the iMS508 model do not indicate growth for the substrates L-Proline, L-Arginine, L-Histidine, L-Ornithine, GABA, Acetate, D-Galactose, D-Xylose, and myo-Inositol, due to the lack of genomic evidence concerning their catabolic pathways. On the other hand, the model published by Gerlin and colleagues [15] includes the necessary reactions, although without any genetic association, which may be valid for *X. fastidiosa* multiplex CFPB 8418 according to the data provided by Biolog Phenotype Microarrays, published alongside the model. Nevertheless, the same behaviour assumption could not be used for the strain used in this work. Not only due to the lack of genomic evidence, but also because other strains do not show growth in media supplemented with L-Histidine, L-Arginine and L-Lysine [58]. Furthermore, it is common for different strains of the same organism to display distinct metabolic behaviours, as shown in *Streptococcus pneumoniae* [33], which can be caused by both genetic diversity and gene regulation. Hence, we assumed that *X. fastidiosa* subsp. *pauca* De Donno was unable to degrade these compounds and the model was reconstructed accordingly.

As stated previously, the presence of a pyrophosphate-dependent phosphofructokinase (EC 2.7.1.90) was identified, allowing the usage of gluconeogenesis by the phytopathogenic organism. However, only the model developed in this work contains this gene-enzyme-reaction association, while in *X. fastidiosa* multiplex CFBP 8418 it was assumed the utilization of this pathway, through the more typical enzyme fructose-1,6-bisphosphate (EC 3.1.3.11) although without any genetic evidence/association to this enzyme.

3.8. Drug Targeting

Drug targeting emerges as one of the most important applications of GSM models. In the past, metabolic models have been used to uncover drug targets for gram-negative pathogens, including *Klebsiella pneumoniae* [14], *Acinetobacter baumannii* [59], and *Pseudomonas aeruginosa* [60]. In this work, drug targeting was achieved through an essentially analysis for both a CHARD2 and an olive media (Supplemental File S5). Moreover, the identified targets were sought in the genome of *O. europaea* using BLAST. A manual pathway analysis was then performed to find alternative routes in the olive tree's metabolism, thus ensuring a minimal effect of the drug in the host.

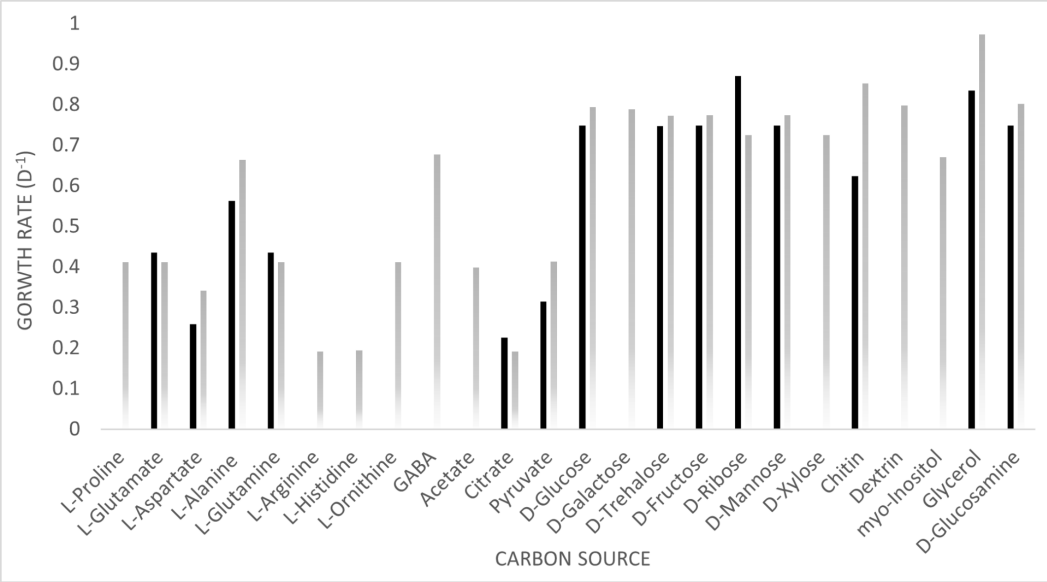

Figure 3. Comparison of *X. fastidiosa*'s GSM models growth rate (d^{-1}) predictions under different carbon sources. The lack of growth prediction in some carbon sources by the *X. fastidiosa pauca* De Donno GSM model is justified by the lack of genomic evidence for enzymes related to the catabolic pathways of the metabolites, while the other model included these catabolic reactions without any gene association.

The discovered drug targets were mapped to known drugs that have documented inhibitory effects on the gene. As expected, antibiotics represented the majority of the found drugs, affecting the peptidoglycan and cell wall assembly (Table S3). More specifically, penicillin-binding proteins (PBP) antibiotics were the most represented class of drugs identified. Besides genes encoding such proteins, seven genes were also identified as potential drug targets, and 11 drugs linked to such genes (Table 5).

B9J09_RS07720 and B9J09_RS10475 are linked to peptidoglycan biosynthesis. These genes encode a UDP-N-acetylglucosamine 1-carboxyvinyltransferase (murA) and D-Alanine-D-alanine ligase, respectively. Fosfomycin was identified as an inhibitor of the former. This drug represents a broad-spectrum antibiotic produced by *Streptomyces species*and has been proven effective against gram-negative bacteria, including *E. coli*, *A. baumannii*, and *P. aeruginosa*. The mechanism of action for Fosfomycin is the irreversible inhibition of the enzyme by binding covalently to a cysteine in the active site of the murA enzyme. Hence, UDP-N-acetylmuramic, which is a precursor for peptidoglycan production, is not produced, and the cell wall synthesis disrupted. *Chlamydia trachomatis* has been shown to be resistant to this antibiotic due to the exchange of cysteine by aspartate in the active site. Still, the genome of *X. fastidiosa* indicates the presence of a cysteine in the murA gene (Figure S2), this drug could potentially be used against this phytopathogen. For the B9J09_RS10475 gene, the identified inhibition drug was Cycloserine, which was also identified for the alanine racemase target (encoded by B9J09_RS10245). However, resistance against this drug was already shown for *X. fastidiosa* [61]. The resistance mechanism against cycloserine has been proposed to be associated with an increase in the expression of alanine racemase in *Streptococci* [62]. More complex mechanisms, that involve mutations in 16 genes, have been proposed recently for the cycloserine resistant *Mycobacterium tuberculosis* [63].

Dihydrofolate reductase, encoded by the B9J09_RS03350 gene, is responsible for the synthesis of tetrahydrofolate. Seven different drugs were identified for this target, of which, only Trimethoprim seems to have reports of resistance in *X. fastidiosa* [64]. The resistance mechanisms in *E. coli* is associated with efflux pumps, such as the multidrug resistance protein MdtK [62]. Based on BLAST alignments, one multidrug efflux pump was identified in the genome of *X. fastidiosa*: *B9J09_RS11465*. The protein encoded by this gene was

Table 5. Potential drug targets evaluated for CHARD2 and Olive medium. The data was retrieved from the DrugBank database, considering only drugs with known inhibitory or antagonistic effects.

Locus Tag	EC number(s)	Pathways	Drugs
B9J09_RS00150	2.6.1.107, 2.6.1.57	Aminoacids	Adapalene
B9J09_RS03245	2.4.2.8	Nucleotide	Mercaptopurine
B9J09_RS07720	2.5.1.7	Peptidoglycan	Fosfomycin
B9J09_RS10475	6.3.2.4	Peptidoglycan	Cycloserine
B9J09_RS07345	1.8.1.2	Sulfur Metabolism	Pimagedine Miconazole Minocycline Lipoic acid Methylene blue Ketamine
B9J09_RS10245	5.1.1.1	Amino acids	Cycloserine
B9J09_RS03350	1.5.1.3	Cofactors	Trimethoprim Methotrexate Trimetrexate Pemetrexed Pyrimethamine Pralatrexate Aminopterin
B9J09_RS04800	2.1.2.3; 3.5.4.10	Nucleotide	Methotrexate
B9J09_RS08730	1.17.4.1	Nucleotide	Gemcitabine
B9J09_RS08735	1.17.4.1	Nucleotide	Hydroxyurea
B9J09_RS10510	3.4.16.4	Peptidoglycan	Carbenicillin Ampicillin
B9J09_RS10095	3.4.16.4, 2.4.1.129	Peptidoglycan	Carbenicillin Cephaloridine Ampicillin
B9J09_RS01610	3.4.16.4, 2.4.1.129	Peptidoglycan	Carbenicillin Cephaloridine
B9J09_RS10110	3.4.16.4	Peptidoglycan	Carbenicillin
B9J09_RS08160	3.4.16.4	Peptidoglycan	Carbenicillin
B9J09_RS06765	3.4.16.4	Peptidoglycan	Carbenicillin
B9J09_RS03770	3.4.16.4	Peptidoglycan	Carbenicillin
B9J09_RS10490	2.4.1.129	Peptidoglycan	Carbenicillin
B9J09_RS06250	2.4.1.129	Peptidoglycan	Carbenicillin
B9J09_RS08155	2.4.1.129	Peptidoglycan	Carbenicillin

annotated as a Na^+/ drug antiporter that confers resistance to several drugs, homologous to the NorM protein identified in *Vibrio parahaemolyticus*. Furthermore, Hydroxyurea was successfully shown to inhibit ribonucleoside-diphosphate reductase in *E. coli* [65]. As for PBP, they are a widely used target for antibiotics. They have a key role in cell wall assembly, which is crucial for virulent pathogens. Using EC number analyses (3.4.16.4 and 2.4.1.129) and BLAST alignments, 61 different antibiotics targeting PBP were classified as potential drugs for *X. fastidiosa*. Antibiotic screening has already shown susceptibility of *X. fastidiosa* against some of the identified drugs, such as cephaloridine, cephaloglycin, carbenicillin, and ampicillin [61]. Carbenicillin was identified as potential drug target for 10 PBPs. Nevertheless, the resistance of *X. fastidiosa* to this antibiotic appears to be strain-dependent, as different susceptibility was detected in different strains: *X. fastidiosa* subps. *pauca* subsp. nov. and *X. fastidiosa* subps. *multiplex* subsp. nov. were identified as carbenicillin-resistant, while *X. fastidiosa* subps. *piercei* is susceptible [66]. Analysing the genomes of these strains would be useful to study the resistance mechanisms of *X. fastidiosa* against this antibiotic.

In future work, the prediction capabilities of the iMS508 model towards specific drugs could be improved by integrating drug resistance mechanisms and using complementary methods such as machine learning algorithms [67]. These mechanisms could include antibiotics degrading enzymes, multi-drug resistance efflux pumps, and gene regulation and expression data.

4. Conclusions

The output of this work was the reconstruction of a GSM model for *X. fastidiosa* subsp. *pauca* De Donno, named iMS508. The model was reconstructed using *merlin*, using an automatic genome annotation approach. Biological databases were also considered during the process of retrieving relevant information. The iMS508 metabolic model has 508 genes, 1285 metabolites, 1164 reactions, and 3 compartments. The model was successfully validated accordingly to the aerobic metabolism, flux through oxidative phosphorylation complexes, auxotrophies and glucose flux pattern. Moreover, it was able to simulate aerobic growth of the bacterium and accurately predict production rates of fastidian gum and the lesA protein. Moreover, the model was also used for drug target identification revealing in total 20 potential drug targets, mostly penicillin-binding proteins. Genes not considered critical in the olive tree were mapped to drugs that had an inhibitory effect, revealing 11 drugs that could potentially be used against this phytopathogen.

Supplementary Materials: The following supporting information can be downloaded at: https://www.mdpi.com/article/10.3390/1010000/s1, Figure S1: Automatic workflow employed; Figure S2: murA aminoacid sequence; Table S1: Detailed biomass composition of *X. fastidiosa pauca* De Donno; Table S2: Genome annotation results; Table S3: Complete list of drugs known to inhibit the found targets.

Author Contributions: Conceptualization: AO, EC, MS, CF, and OD; Data curation: AO, EC, and MS; Formal analysis: AO, EC, and MS; Methodology: AO, EC, MS, CF, and OD; Supervision: OD and CF; Validation: AO, EC; Writing - original draft: AO and EC; Writing - review & editing: OD and CF

Funding: This study was supported by the Portuguese Foundation for Science and Technology (FCT) under the scope of the strategic funding of UIDB/04469/2020 unit. A. Oliveira (DFA/BD/10205/2020), E. Cunha (DFA/BD/8076/2020) hold a doctoral fellowship provided by the FCT. Oscar Dias acknowledges FCT for the Assistant Research contract obtained under CEEC Individual 2018.

Data Availability Statement: The model presented in this work can be found in BioModels with the identifier MODEL2205020002.

Acknowledgments: We would like to acknowledge the Portuguese Foundation for Science and Technology for supporting this work.

Conflicts of Interest: The authors declare that there is no conflict of interest in this study.

Abbreviations

The following abbreviations are used in this manuscript:

BLAST	Basic Local Alignment Search Tool
EMP	Entner-Doudoroff pathway
GSM	Genome-scale metabolic
I2P2	Impact Indicator for Priority Pests
merlin	Metabolic Models Reconstruction Using Genome-Scale Information
PBP	Penicillin-Binding Protein
ROS	Reactive Oxygen Species
SBML	Systems Biology Markup Language

References

1. Wells, J.M.; Raju, B.C.; Hung, H.Y.; Weisburg, W.G.; Mandelco-Paul, L.; Brenner, D.J. *Xylella fastidiosa* gen. nov. , sp. nov: Gram-Negative, Xylem- Limited, Fastidious Plant Bacteria Related to *Xanthomonas* spp. *International Journal of Systematic Bacteriology* **1987**, *37*, 136–143. https://doi.org/10.1099/00207713-37-2-136.

2. Chatterjee, S.; Almeida, R.P.P.; Lindow, S. Living in two Worlds: The Plant and Insect Lifestyles of *Xylella fastidiosa*. *Annual Review of Phytopathology* **2008**, *46*, 243–271. https://doi.org/10.1146/annurev.phyto.45.062806.094342.
3. Bradbury, J. *Guide to Plant Pathogenic Bacteria*; CAB International Mycological Institute, 1986.
4. (EFSA), E.F.S.A. Update of the *Xylella* spp . host plant database, 2018. https://doi.org/10.2903/j.efsa.2018.5408.
5. Nunney, L.; Vickerman, D.B.; Bromley, R.E.; Russell, S.A.; Hartman, J.R.; Morano, L.D.; Stouthamer, R. Recent Evolutionary Radiation and Host Plant Specialization in the *Xylella fastidiosa* Subspecies Native to the United States. *Applied and Environmental Microbiology* **2013**, *79*, 2189–2200. https://doi.org/10.1128/AEM.03208-12.
6. Baldi, P.; Porta, N.L. *Xylella fastidiosa* : Host Range and Advance in Molecular Identification Techniques. *Frontiers in Plant Science* **2017**, *8*, 1–22. https://doi.org/10.3389/fpls.2017.00944.
7. Elbeaino, T.; Valentini, F.; Abou Kubaa, R.; Moubarak, P.; Yaseen, T.; Digiaro, M. Multilocus sequence typing of *Xylella fastidiosa*; isolated from olive affected by "olive quick decline syndrome" in Italy. *Phytopathologia Mediterranea* **2014**, *53*, 533–542. https://doi.org/10.14601/Phytopathol_Mediterr-15000.
8. Saponari, M.; Giampetruzzi, A.; Loconsole, G.; Boscia, D.; Saldarelli, P. *Xylella fastidiosa* in olive in Apulia: where we stand. *Phytopathology* **2018**, pp. 1–43. https://doi.org/10.1094/PHYTO-08-18-0319-FI.
9. Schneider, K.; van der Werf, W.; Cendoya, M.; Mourits, M.; Navas-Cortés, J.A.; Vicent, A.; Lansink, A.O. Impact of *Xylella fastidiosa* subspecies *pauca* in European olives. *Proceedings of the National Academy of Sciences* **2020**, *117*, 9250–9259. https://doi.org/10.1073/pnas.1912206117.
10. Vos, S.; Camilleri, M.; Diakaki, M.; Lázaro, E.; Parnell, S.; Schrader, G.; Vicent, A. Pest survey card on *Xylella fastidiosa*. *EFSA Supporting Publications* **2019**. https://doi.org/10.2903/sp.efsa.2019.EN-1667.
11. Palsson, B. *Systems Biology - Properties of Reconstructed Networks*; 2006.
12. Dias, O.; Rocha, I., Systems biology in fungi. In *Molecular Biology of Food and Water Borne Mycotoxigenic and Mycotic Fungi*; CRC Press Boca Raton, 2015; pp. 69–92.
13. Presta, L.; Bosi, E.; Mansouri, L.; Dijkshoorn, L.; Fani, R.; Fondi, M. Constraint-based modeling identifies new putative targets to fight colistin-resistant *A. baumannii* infections. *Scientific Reports* **2017**, *7*, 3706. https://doi.org/10.1038/s41598-017-03416-2.
14. Cesur, M.F.; Siraj, B.; Uddin, R.; Durmuş, S.; Çakır, T. Network-Based Metabolism-Centered Screening of Potential Drug Targets in *Klebsiella pneumoniae* at Genome Scale. *Frontiers in cellular and infection microbiology* **2019**, *9*, 447. https://doi.org/10.3389/fcimb.2019.00447.
15. Gerlin, L.; Cottret, L.; Cesbron, S.; Taghouti, G.; Jacques, M.A.; Genin, S.; Baroukh, C. Genome-Scale Investigation of the Metabolic Determinants Generating Bacterial Fastidious Growth. *mSystems* **2020**, *5*, 1–15. https://doi.org/10.1128/mSystems.00698-19.
16. Capela, J.; Lagoa, D.; Rodrigues, R.; Cunha, E.; Cruz, F.; Barbosa, A.; Bastos, J.; Lima, D.; Ferreira, E.C.; Rocha, M.; et al. merlin, an improved framework for the reconstruction of high-quality genome-scale metabolic models. *Nucleic Acids Research* **2022**, *50*, 6052–6066. https://doi.org/10.1093/nar/gkac459.
17. Ebrahim, A.; Lerman, J.A.; Palsson, B.O.; Hyduke, D.R. COBRApy: constraints-based reconstruction and analysis for python. *BMC systems biology* **2013**, *7*, 1–6. https://doi.org/10.1186/1752-0509-7-74.
18. Cock, P.J.A.; Antao, T.; Chang, J.T.; Chapman, B.A.; Cox, C.J.; Dalke, A.; Friedberg, I.; Hamelryck, T.; Kauff, F.; Wilczynski, B.; et al. Biopython: freely available Python tools for computational molecular biology and bioinformatics. *Bioinformatics* **2009**, *25*, 1422–1423. https://doi.org/10.1093/bioinformatics/btp163.
19. Sayers, E.W.; Bolton, E.E.; Brister, J.R.; Canese, K.; Chan, J.; Comeau, D.; Connor, R.; Funk, K.; Kelly, C.; Kim, S.; et al. Database resources of the national center for biotechnology information. *Nucleic Acids Research* **2022**, *50*, D20–D26. https://doi.org/10.1093/NAR/GKAB1112.
20. Giampetruzzi, A.; Saponari, M.; Almeida, R.P.P.; Essakhi, S.; Boscia, D.; Loconsole, G.; Saldarelli, P. Complete Genome Sequence of the Olive-Infecting Strain *Xylella fastidiosa* subsp. *pauca* De Donno. *Genome Announcements* **2017**, *5*, 5–6. https://doi.org/10.1128/genomeA.00569-17.
21. Altschul, S.F.; Gish, W.; Miller, W.; Myers, E.W.; Lipman, D.J. Basic local alignment search tool. *Journal of Molecular Biology* **1990**, *215*, 403–410. https://doi.org/10.1016/S0022-2836(05)80360-2.
22. Enzyme nomenclature 1992 : recommendations of the Nomenclature Committee of the International Union of Biochemistry and Molecular Biology on the nomenclature and classification of enzymes : International Union of Biochemistry and Molecular Biology. Nomenclature Committee, author : Free Download, Borrow, and Streaming : Internet Archive.
23. Kanehisa, M.; Furumichi, M.; Tanabe, M.; Sato, Y.; Morishima, K. KEGG: new perspectives on genomes, pathways, diseases and drugs. *Nucleic Acids Research* **2016**, *45*, D353–D361. https://doi.org/10.1093/nar/gkw1092.
24. Yu, N.Y.; Wagner, J.R.; Laird, M.R.; Melli, G.; Rey, S.; Lo, R.; Dao, P.; Sahinalp, S.C.; Ester, M.; Foster, L.J.; et al. PSORTb 3.0: improved protein subcellular localization prediction with refined localization subcategories and predictive capabilities for all prokaryotes. *Bioinformatics* **2010**, *26*, 1608–1615. https://doi.org/10.1093/bioinformatics/btq249.
25. Saier, M.H.; Reddy, V.S.; Tsu, B.V.; Ahmed, M.S.; Li, C.; Moreno-Hagelsieb, G. The Transporter Classification Database (TCDB): recent advances. *Nucleic Acids Research* **2016**, *44*, D372–D379. https://doi.org/10.1093/nar/gkv1103.
26. Orth, J.D.; Conrad, T.M.; Na, J.; Lerman, J.A.; Nam, H.; Feist, A.M.; Palsson, B.Ø. A comprehensive genome-scale reconstruction of *Escherichia coli* metabolism. *Molecular Systems Biology* **2011**, *7*, 1–9. https://doi.org/10.1038/msb.2011.65.

27. Schatschneider, S.; Persicke, M.; Watt, S.A.; Hublik, G.; Pühler, A.; Niehaus, K.; Vorhölter, F.J. Establishment, *in silico* analysis, and experimental verification of a large-scale metabolic network of the xanthan producing *Xanthomonas campestris* pv. campestris strain B100. *Journal of Biotechnology* **2013**, *167*, 123–134. https://doi.org/10.1016/j.jbiotec.2013.01.023.
28. Santos, S.; Rocha, I. Estimation of biomass composition from genomic and transcriptomic information. *Journal of Integrative Bioinformatics* **2016**, *13*, 1–14. https://doi.org/10.1515/jib-2016-285.
29. Vollmer, W.; Holtje, J.V. The Architecture of the Murein (Peptidoglycan) in Gram-Negative Bacteria : Vertical Scaffold or Horizontal Layer (s)? *Journal of Bacteriology* **2004**, *186*, 5978–5987. https://doi.org/10.1128/JB.186.18.5978.
30. Wang, X.; Quinn, P.J. Lipopolysaccharide: Biosynthetic pathway and structure modification. *Progress in Lipid Research* **2010**, *49*, 97–107. https://doi.org/10.1016/j.plipres.2009.06.002.
31. Whitfield, C. Biosynthesis of lipopolysaccharide O antigens. *Trends in Microbiology* **1995**, *3*, 178–185. https://doi.org/10.1016/s0966-842x(00)88917-9.
32. Dianese, J.C.; Schaad, N.W. Isolation and Characterization of Inner and Outer Membranes of *Xanthomonas campestris* pv. campestris. *Phytopathology* **1982**, *72*, 1284–1289. https://doi.org/10.1128/jb.176.11.3354-3359.1994.
33. Dias, O.; Saraiva, J.; Faria, C.; Ramirez, M.; Pinto, F.; Rocha, I. iDS372, a Phenotypically Reconciled Model for the Metabolism of Streptococcus pneumoniae Strain R6. *Frontiers in Microbiology* **2019**, *10*. https://doi.org/10.3389/fmicb.2019.01283.
34. Ma, H.; Zeng, A.P. Reconstruction of metabolic networks from genome data and analysis of their global structure for various organisms. *Bioinformatics* **2003**, *19*, 270–277, [https://academic.oup.com/bioinformatics/article-pdf/19/2/270/1059951/190270.pdf]. https://doi.org/10.1093/bioinformatics/19.2.270.
35. Cruz, F.; Capela, J.; Ferreira, E.C.; Rocha, M.; Dias, O. BioISO: an objective-oriented application for assisting the curation of genome-scale metabolic models. *bioRxiv* **2021**, [https://www.biorxiv.org/content/early/2021/03/12/2021.03.07.434259.full.pdf]. https://doi.org/10.1101/2021.03.07.434259.
36. Lewis, N.E.; Hixson, K.K.; Conrad, T.M.; Lerman, J.A.; Charusanti, P.; Polpitiya, A.D.; Adkins, J.N.; Schramm, G.; Purvine, S.O.; Lopez-Ferrer, D.; et al. Omic data from evolved *E. coli* are consistent with computed optimal growth from genome-scale models. *Molecular systems biology* **2010**, *6*, 390. https://doi.org/10.1038/msb.2010.47.
37. Frese, M.; Schatschneider, S.; Voss, J.; Vorhölter, F.J.; Niehaus, K. Characterization of the pyrophosphate-dependent 6-phosphofructokinase from *Xanthomonas campestris* pv. campestris. *Archives of Biochemistry and Biophysics* **2014**, *546*, 53–63. https://doi.org/10.1016/j.abb.2014.01.023.
38. Schatschneider, S.; Huber, C.; Neuweger, H.; Watt, T.F.; Pühler, A.; Eisenreich, W.; Wittmann, C.; Niehaus, K.; Vorhölter, F.J. Metabolic flux pattern of glucose utilization by *Xanthomonas campestris* pv . campestris : prevalent role of the Entner – Doudoroff pathway and minor fluxes through the pentose phosphate pathway and glycolysis. *Molecular BioSystems* **2014**, *10*, 2663–2676. https://doi.org/10.1039/C4MB00198B.
39. Letisse, F.; Chevallereau, P.; Simon, J.L.; Lindley, N.D. Kinetic analysis of growth and xanthan gum production with *Xanthomonas campestris* on sucrose, using sequentially consumed nitrogen sources. *Applied Microbiology and Biotechnology* **2001**, *55*, 417–422. https://doi.org/10.1007/s002530000580.
40. Nascimento, R.; Gouran, H.; Chakraborty, S.; Gillespie, H.W.; Almeida-Souza, H.O.; Tu, A.; Rao, B.J.; Feldstein, P.A.; Bruening, G.; Goulart, L.R.; et al. The Type II Secreted Lipase/Esterase LesA is a Key Virulence Factor Required for *Xylella fastidiosa* Pathogenesis in Grapevines. *Scientific Reports* **2016**, *6*, 1–17. https://doi.org/10.1038/srep18598.
41. Drossopoulos, J.; Niavis, C. Seasonal changes of the metabolites in the leaves, bark and xylem tissues of olive tree (*Olea europaea*. L) I. Nitrogenous compounds. *Annals of botany* **1988**, *62*, 313–320. https://doi.org/10.1093/oxfordjournals.aob.a087663.
42. Leite, B.; Andersen, P.C.; Ishida, M.L. Colony aggregation and biofilm formation in xylem chemistry-based media for *Xylella fastidiosa*. *FEMS Microbiology Letters* **2004**, *230*, 283–290. https://doi.org/10.1016/S0378-1097(03)00917-0.
43. Wishart, D.S.; Wu, A. Using DrugBank for *In Silico* Drug Exploration and Discovery. *Current Protocols in Bioinformatics* **2016**, *54*, 14.4.1–14.4.31. https://doi.org/10.1002/CPBI.1.
44. Chang, A.; Jeske, L.; Ulbrich, S.; Hofmann, J.; Koblitz, J.; Schomburg, I.; Neumann-Schaal, M.; Jahn, D.; Schomburg, D. BRENDA, the ELIXIR core data resource in 2021: new developments and updates. *Nucleic Acids Research* **2021**, *49*, D498–D508. https://doi.org/10.1093/nar/gkaa1025.
45. Henrissat, B.; Deleury, E.; Coutinho, P.M. Glycogen metabolism loss: a common marker of parasitic behaviour in bacteria? *Trends in Genetics* **2002**, *18*, 437–440. https://doi.org/10.1016/S0168-9525(02)02734-8.
46. Pielken, P.; Schimz, K.L.; Eggeling, L.; Sahm, H. Glucose metabolism in *Xanthomonas campestris* and influence of methionine on the carbon flow. *Canadian Journal of Microbiology* **1988**, *34*, 1333–1337. https://doi.org/10.1139/m88-234.
47. Lemos, E.G.d.M.; Alves, L.M.C.; Campanharo, J.C. Genomics-based design of defined growth media for the plant pathogen *Xylella fastidiosa*. *FEMS Microbiology Letters* **2003**, *219*, 39–45. https://doi.org/10.1016/S0378-1097(02)01189-8.
48. Malik-Sheriff, R.S.; Glont, M.; Nguyen, T.V.N.; Tiwari, K.; Roberts, M.G.; Xavier, A.; Vu, M.T.; Men, J.; Maire, M.; Kananathan, S.; et al. BioModels — 15 years of sharing computational models in life science. *Nucleic Acids Research* **2020**, *48*, D407–D415. https://doi.org/10.1093/nar/gkz1055.
49. Hucka, M.; Bergmann, F.T.; Dräger, A.; Hoops, S.; Keating, S.M.; Novère, N.L.; Myers, C.J.; Olivier, B.G.; Sahle, S.; Schaff, J.C.; et al. The Systems Biology Markup Language (SBML): Language Specification for Level 3 Version 2 Core. *Journal of Integrative Bioinformatics* **2018**, *15*, 20170081. https://doi.org/doi:10.1515/jib-2017-0081.

50. Zagallo, A.C.; Wang, C.H. Comparative Glucose Catabolism of *Xanthomonas* Species. *Journal of Bacteriology* **1967**, *93*, 970–975. https://doi.org/10.1128/jb.93.3.970-975.1967.
51. Facincani, A.P.; Ferro, J.A.; Jr., J.M.P.; Jr., H.A.P.; de Macedo Lemos, E.G.; do Prado, A.L.; Ferro, M.I.T. Carbohydrate metabolism of *Xylella fastidiosa*: Detection of glycolytic and pentose phosphate pathway enzymes and cloning and expression of the enolase gene. *Genetics and Molecular Biology* **2003**, *26*, 203–211. https://doi.org/10.1590/S1415-47572003000200015.
52. O'Brien, J.A.; Daudi, A.; Butt, V.S.; Bolwell, G.P. Reactive oxygen species and their role in plant defence and cell wall metabolism. *Planta* **2012**, *236*, 765–779. https://doi.org/10.1007/s00425-012-1696-9.
53. Hijaz, F.; Killiny, N. Collection and Chemical Composition of Phloem Sap from Citrus sinensis *L. Osbeck* (Sweet Orange). *PLOS ONE* **2014**, *9*, 1–11. https://doi.org/10.1371/journal.pone.0101830.
54. Bailey-Serres, J.; Mittler, R. The Roles of Reactive Oxygen Species in Plant Cells. *Plant Physiology* **2006**, *141*, 311. https://doi.org/10.1104/pp.104.900191.
55. Chavarría, M.; Nikel, P.I.; Pérez-pantoja, D.; Lorenzo, V.D.; José, S.; Rica, C. The Entner – Doudoroff pathway empowers *Pseudomonas putida* KT2440 with a high tolerance to oxidative stress. *Environmental Microbiology* **2013**, *15*, 1772–1785. https://doi.org/10.1111/1462-2920.12069.
56. Poplawsky, A.R.; Urban, S.C.; Chun, W. Biological Role of Xanthomonadin Pigments in *Xanthomonas campestris* pv. Campestris. *Applied and Environmental Microbiology* **2000**, *66*, 5123–5127. https://doi.org/10.1128/AEM.66.12.5123-5127.2000.
57. Zhou, L.; Wang, J.Y.; Wang, J.; Poplawsky, A.; Lin, S.; Zhu, B.; Chang, C.; Zhou, T.; Zhang, L.H.; He, Y.W. The diffusible factor synthase XanB2 is a bifunctional chorismatase that links the shikimate pathway to ubiquinone and xanthomonadins biosynthetic pathways. *Molecular Microbiology* **2013**, *87*, 80–93. https://doi.org/10.1111/mmi.12084.
58. Chang, C.J.; Donaldson, R.C. Nutritional requirements of *Xylella fastidiosa*, which causes Pierce's disease in grapes. *Canadian Journal of Microbiology* **2000**, *46*, 291–293. https://doi.org/10.1139/w99-141.
59. Kim, H.U.; Kim, T.Y.; Lee, S.Y. Genome-scale metabolic network analysis and drug targeting of multi-drug resistant pathogen *Acinetobacter baumannii* AYE. *Molecular BioSystems* **2010**, *6*, 339–348. https://doi.org/10.1039/b916446d.
60. Bartell, J.A.; Blazier, A.S.; Yen, P.; Thøgersen, J.C.; Jelsbak, L.; Goldberg, J.B.; Papin, J.A. Reconstruction of the metabolic network of *Pseudomonas aeruginosa* to interrogate virulence factor synthesis. *Nature Communications 2017 8:1* **2017**, *8*, 1–13. https://doi.org/10.1039/b916446d.
61. Bleve, G.; Gallo, A.; Altomare, C.; Vurro, M.; Maiorano, G.; Cardinali, A.; D'Antuono, I.; Marchi, G.; Mita, G. *In vitro* activity of antimicrobial compounds against *Xylella fastidiosa*, the causal agent of the olive quick decline syndrome in Apulia (Italy). *FEMS Microbiology Letters* **2018**, *365*, 281. https://doi.org/10.1093/femsle/fnx281.
62. Reitz, R.H.; Slade, H.D.; Neuhaus, F.C. The Biochemical Mechanisms of Resistance by Streptococci to the Antibiotics D-Cycloserine and O-Carbamyl-D-serine. *Biochemistry* **1967**, *6*, 2561–2570. https://doi.org/10.1021/BI00860A038/ASSET/BI00860A038.FP.PNG_V03.
63. Chen, J.; Zhang, S.; Cui, P.; Shi, W.; Zhang, W.; Zhang, Y. Identification of novel mutations associated with cycloserine resistance in Mycobacterium tuberculosis. *Journal of Antimicrobial Chemotherapy* **2017**, *72*, 3272–3276. https://doi.org/10.1093/jac/dkx316.
64. de P. M. A. Ribeiro, M.; de T. F. Dellias, M.; Tsai, S.M.; Bolmströn, A.; Meinhardt, L.W.; de M. Bellato, C. Utilization of the Etest Assay for Comparative Antibiotic Susceptibility Profiles of Citrus Variegated Chlorosis and Pierce's Disease Strains of *Xylella fastidiosa*. *Current Microbiology* **2005**, *51*, 262–266. https://doi.org/10.1007/s00284-005-0015-0.
65. KJØLLER LARSEN, I.; SJÖOBERG, B..M.; THELANDER, L. Characterization of the Active Site of Ribonucleotide Reductase of *Escherichia coli*, Bacteriophage T4 and Mammalian Cells by Inhibition Studies with *Hydroxyurea Analogues*. *European Journal of Biochemistry* **1982**, *125*, 75–81. https://doi.org/10.1111/j.1432-1033.1982.tb06653.x.
66. Schaad, N.W.; Postnikova, E.; Lacy, G.; Fatmi, M.; Chang, C.J. Xylella fastidiosa subspecies: X. fastidiosa subsp piercei, subsp. nov., X. fastidiosa subsp. multiplex subsp. nov., and X. fastidiosa subsp. pauca subsp. nov. *Systematic and Applied Microbiology* **2004**, *27*, 290–300. https://doi.org/10.1078/0723-2020-00263.
67. Pearcy, N.; Hu, Y.; Baker, M.; Maciel-Guerra, A.; Xue, N.; Wang, W.; Kaler, J.; Peng, Z.; Li, F.; Dottorini, T. Genome-Scale Metabolic Models and Machine Learning Reveal Genetic Determinants of Antibiotic Resistance in Escherichia coli and Unravel the Underlying Metabolic Adaptation Mechanisms. *mSystems* **2021**, *6*, e00913–20, [https://journals.asm.org/doi/pdf/10.1128/mSystems.00913-20]. https://doi.org/10.1128/mSystems.00913-20.

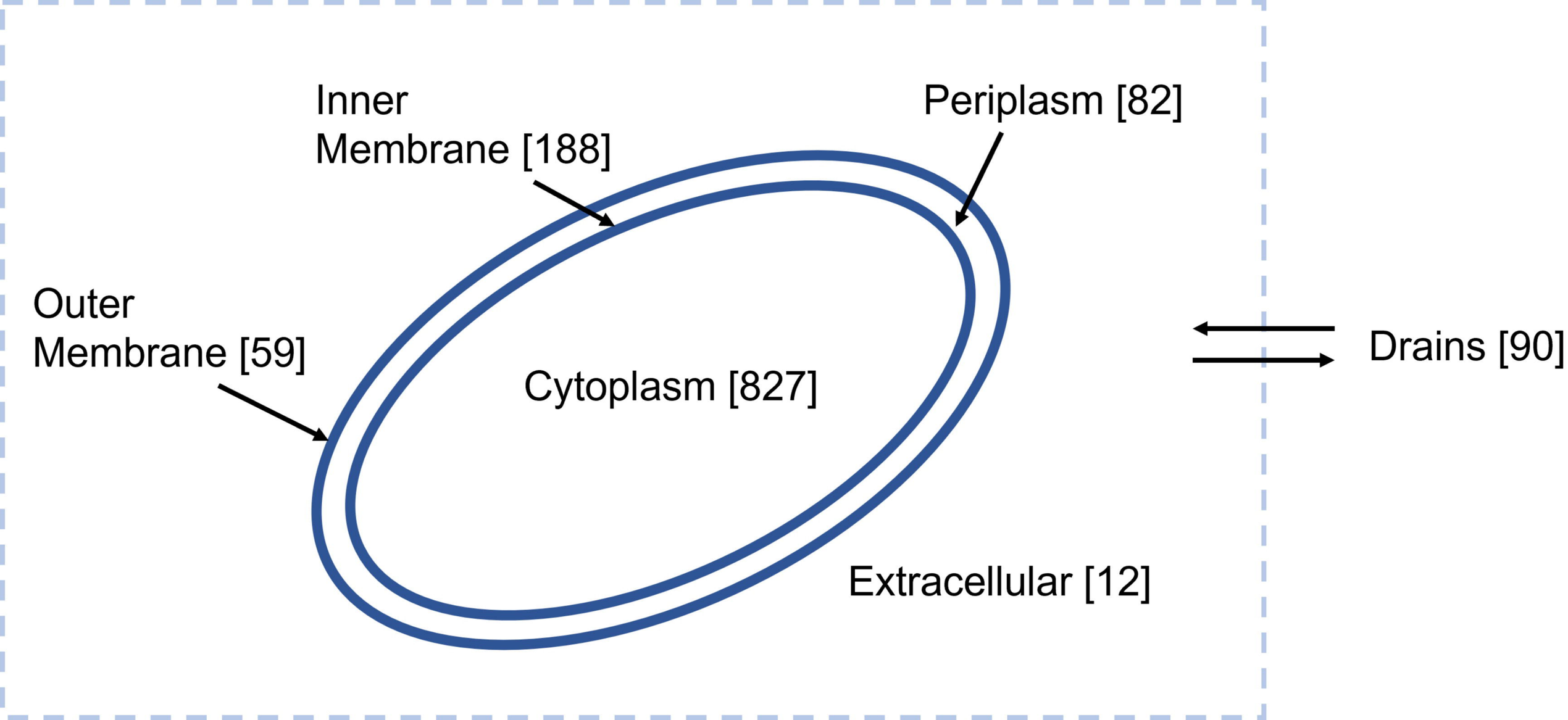
Inner
Membrane [188]
Periplasm [82]
Outer
Membrane [59]
Cytoplasm [827]
Drains [90]
Extracellular [12]

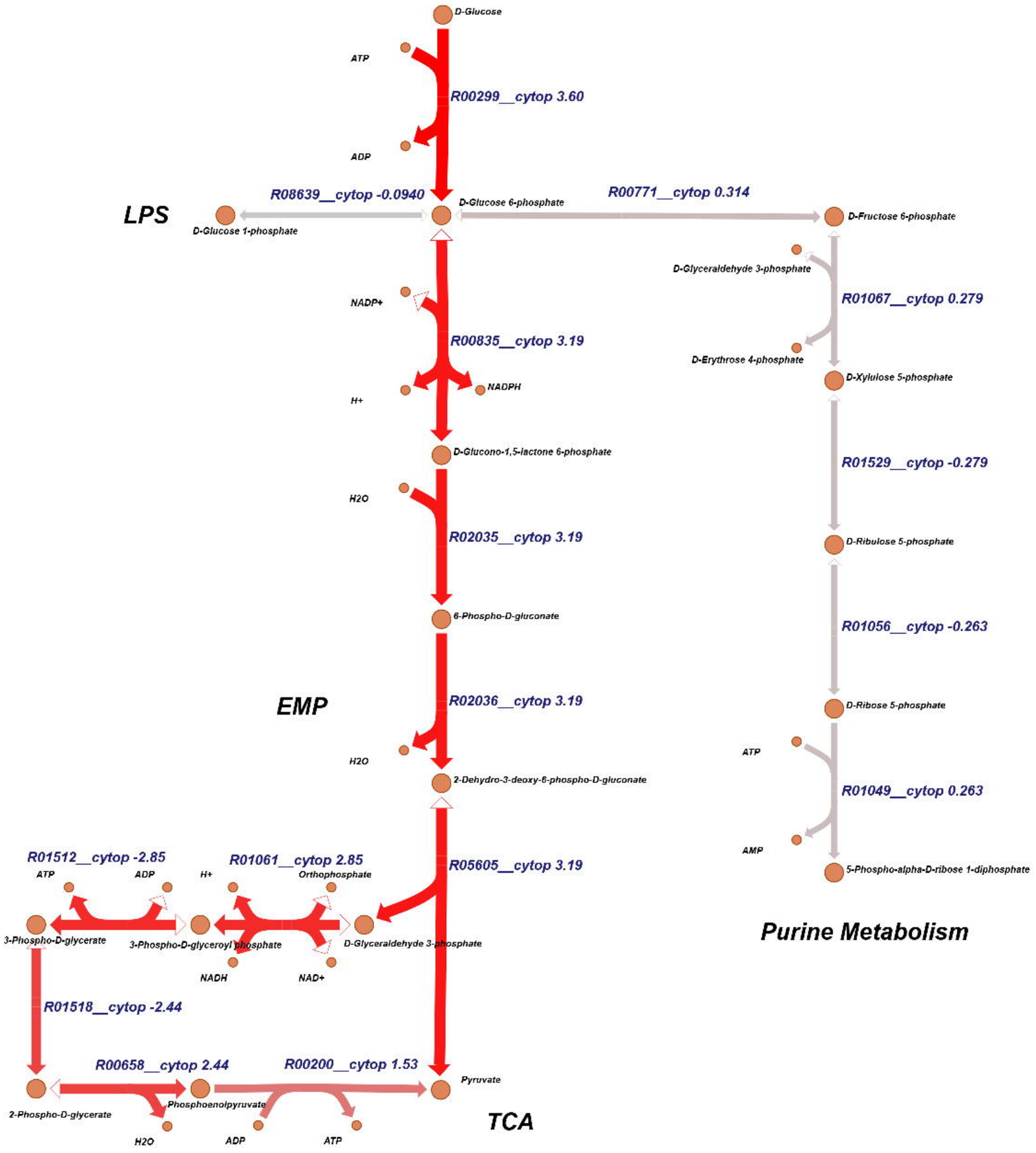
D-Glucose
ATP
R00299__cytop 3.60
ADP
R08639__cytop -0.0940
D-Glucose 6-phosphate
R00771__cytop 0.314
LPS
D-Glucose 1-phosphate
D-Fructose 6-phosphate
D-Glyceraldehyde 3-phosphate
NADP+
R01067__cytop 0.279
R00835__cytop 3.19
D-Erythrose 4-phosphate
D-Xylulose 5-phosphate
NADPH
H+
D-Glucono-1,5-lactone 6-phosphate
R01529__cytop -0.279
H2O
R02035__cytop 3.19
D-Ribulose 5-phosphate
6-Phospho-D-gluconate
R01056__cytop -0.263
EMP
R02036__cytop 3.19
D-Ribose 5-phosphate
H2O
ATP
2-Dehydro-3-deoxy-6-phospho-D-gluconate
R01049__cytop 0.263
AMP
R01512__cytop -2.85
R01061__cytop 2.85
R05605__cytop 3.19
5-Phospho-alpha-D-ribose 1-diphosphate
ATP
ADP
H+
Orthophosphate
3-Phospho-D-glycerate
3-Phospho-D-glyceroyl phosphate
D-Glyceraldehyde 3-phosphate
Purine Metabolism
NADH
NAD+
R01518__cytop -2.44
R00658__cytop 2.44
R00200__cytop 1.53
Pyruvate
2-Phospho-D-glycerate
Phosphoenolpyruvate
H2O
ADP
ATP
TCA

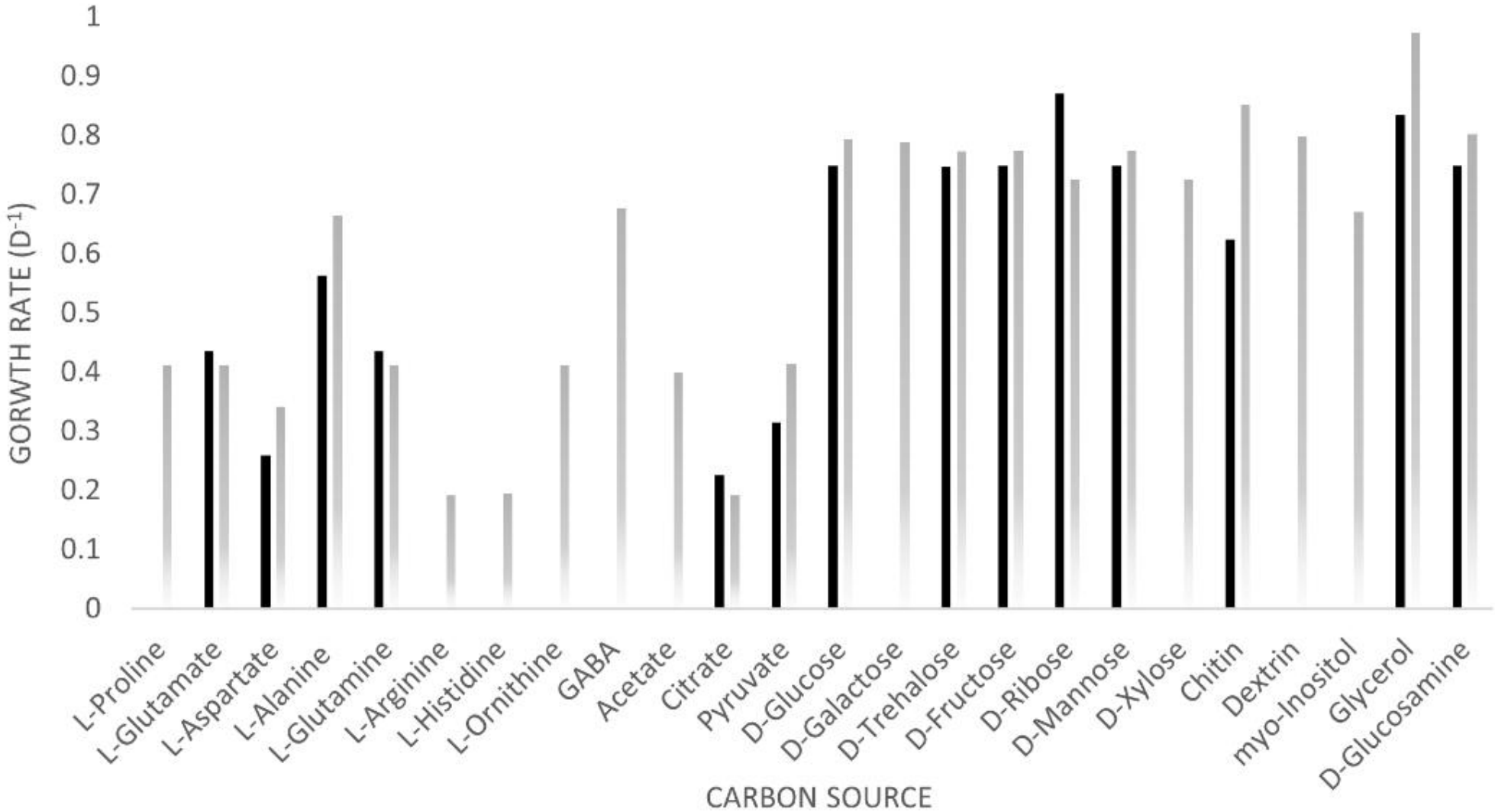
GORWTH RATE (D-1)
1
0.9
0.8
0.7
0.6
0.5
0.4
0.3
0.2
0.1
0
L-Proline
L-Glutamate
L-Aspartate
L-Alanine
L-Glutamine
L-Arginine
L-Histidine
L-Ornithine
GABA
Acetate
Citrate
Pyruvate
D-Glucose
D-Galactose
D-Trehalose
D-Fructose
D-Ribose
D-Mannose
D-Xylose
Chitin
Dextrin
myo-Inositol
Glycerol
D-Glucosamine
CARBON SOURCE